Lights in a sea of darkness: constraining the nature and properties of dark matter using the stellar kinematics in the centres of ultra-faint dwarf galaxies

Zoutendijk, S.L.

1 Introduction

1.1 Cosmology

Throughout history, humans have asked themselves how the world around them came to be, how it is ordered, and how it will change or possibly end. It is clear than these questions are of philosophical importance to many people on Earth. Cosmology is the discipline that concerns itself with these questions. Its name literally means 'the study of the world'. Physical cosmology is the study of the origin, composition, structure, and evolution of our world, the Universe, using the scientific method. In a scientific context, 'physical cosmology' is usually shortened to 'cosmology'; I will do the same in this thesis.

Not only can a scientific approach to cosmology provide answers to important philosophical questions, it can also improve our understanding of fundamental physics[1]. Though science has taught us much about the Universe already, cosmology has revealed that we are still relatively ignorant about the Universe at large. Our working theory of cosmology, the ΛCDM paradigm (Sect. 1.1.1), contains two substances that cannot be explained with established physics. Moreover, several problems have been perceived when comparing ΛCDM to observations at (astronomically) small scales (Sect. 1.1.2). There may be explanations for these problems within the ΛCDM paradigm (Sect. 1.1.3), or without (Sects. 1.1.4 and 1.1.5).

1.1.1 The ΛCDM paradigm

For the past century or so, a revolution in slow motion has been taking place in cosmology. It was a turbulent century for cosmology in general; our picture of the Universe has drastically changed during this period. We learned that 'spiral nebulae' are other galaxies (Hubble, 1929; Oepik, 1922; Shapley & Curtis, 1921), similar to our own Milky Way. We also rewrote fundamental physics with the introduction of special and general relativity (Einstein, 1905c, 1916), and quantum mechanics (e.g. Bohr, 1913; de Broglie, 1925; Einstein, 1905b; Planck, 1901; Schrödinger, 1926). How-

1. To the practically minded reader, I should note that breakthroughs in fundamental physics have often resulted in real-world applications, such as medical imaging, satellite navigation, and faster computing.

ever, the revolution I referred to is the mounting observational evidence for large amounts of dark matter, with which came the slow realization that it is fundamentally different from all the matter we know on Earth. Here I summarize how this evidence was gathered and how it led us to create the ΛCDM paradigm of cosmology. For a more extensive review of the history of dark matter, see Bertone & Hooper (2018).

In the early twentieth century, the first attempts were made to measure the mass of astronomical objects. Contrary to experimental physics, there is no way to directly measure mass in observational astronomy, a science that studies its subjects from afar. However, it was realized that if stars in a galaxy could be treated analogously to particles in a gas, the mass of that galaxy could be inferred from the motions of its stars. I will discuss this in more detail in Sect. 1.4, but the principle is this: If a cloud of gas or a galaxy of stars is to be long-lived, then the motions of its constituent particles or stars need to be balanced by gravity. The system is then said to be in dynamical equilibrium. If the system is not in equilibrium, it will either collapse or fly apart, depending on whether the gravitational potential or the kinetic energy is larger. When the gravitational force required for dynamical equilibrium is calculated from the motions of the stars, the universal law of gravitation (Newton, 1687, p. 412) then yields the mass of the system. This mass is not only that of the stars, glowing gas, and other luminous matter that can be seen through a telescope, but that of all matter, including dark matter.

The first measurements of the velocity dispersion of nearby stars in our own Milky Way Galaxy indicated that there is little dark matter relative to luminous matter in our neighbourhood (e.g. Kapteyn, 1922; Kelvin, 1904; Oort, 1932; Öpik, 1915; Poincaré, 1906). However, observations at larger scales told a different story. The velocity dispersion of galaxies inside galaxy clusters revealed that these clusters were hundreds of times more massive than estimated from their luminosity (e.g. Schwarzschild, 1954; Smith, 1936; Zwicky, 1933). Later, a similar technique was used to estimate the mass of other spiral galaxies from the circular motions of their stars and gas. It was found that these galaxies are also more massive than expected, and that the additional mass is mostly located at large radii, where little luminous matter is seen (e.g. Bosma, 1978; Freeman, 1970; Roberts & Rots, 1973; Rogstad & Shostak, 1972; Rubin et al., 1978). This suggests that the dark matter has a different distribution than the luminous matter, forming a halo around a galaxy, and it was pointed out that the mass discrepancy in galaxies might be connected to that in galaxy clusters (Einasto et al., 1974; Ostriker et al., 1974).

When the astrophysical community became convinced that the Uni-

verse contains much more dark than luminous matter, with different distributions, the next question to answer was what that dark matter could be. In the earliest discussions of dark matter, when there was no evidence yet that it was more abundant than luminous matter, various options were suggested: dark stars, dark nebulae, and planets, comets, and other solid objects (e.g. Kelvin, 1904; Oort, 1932). When the search for dark matter began in earnest, black holes and faint stars such as brown dwarfs, white dwarfs, and neutron stars (together these correspond to the earlier hypothetical concept of dark stars), as well as planets, were popular options, later receiving the collective name of massive astrophysical compact halo objects (MACHOs; Griest, 1991). The MACHOs proposed at the time were made of the same particles as the luminous matter and the matter found on Earth. This kind of matter is called baryonic matter, because it is mostly composed of baryons such as protons and neutrons. The present-day abundance of light elements and isotopes constrains the density of baryons at the time of the formation of these elements, early in the history of the Universe. It was found that only a small fraction of matter and energy[2] in the Universe, about 5%, is composed of baryons (e.g. Burles et al., 2001; Fukugita et al., 1998; Reeves et al., 1973). This means that if dark matter is composed of MACHOs, these MACHOs can in turn not be made of baryons, and are therefore not normal faint stars or black holes. One remaining possibility is that the MACHOs could be black holes that formed before the light elements were created (Carr & Hawking, 1974); these are called primordial black holes (PBHs).

The alternative to MACHOs and currently preferred hypothesis is that dark matter consists of weakly interacting massive particles (WIMPs; Steigman & Turner, 1985). The WIMPs are similarly required to be non-baryonic, and their weak interaction means that they will not form MACHOs such as black holes, stars, and planets.

An early favourite was that the dark matter was some kind of neutrino (e.g. Szalay & Marx, 1976), a class of WIMPs that had already been proven to exist. Ordinary neutrinos turned out to be not a good fit, because they were too light. Simulations showed that the extraordinarily low mass of neutrinos made them so fleeting that they would not condense to form structures similar to those that we observe, but instead would form hazier structures (White et al., 1983). If dark matter is thought of as a gas, the low mass and high velocities would correspond to a high temperature. This

2. Thanks to the theory of special relativity (Einstein, 1905c), we know that matter and energy are equivalent according to $E = mc^2$ (Einstein, 1905a). This equation allows us to compare the matter and energy in the Universe on a single scale.

model is know as hot dark matter (HDM), and is ruled out by the aforementioned simulations. However, it is possible that dark matter consists of a new kind of neutrino, or another new weakly interacting particle, that is much heavier than the neutrinos we know. Such a particle would be cold dark matter (CDM). To be considered cold, the particle needs to have a mass much larger than 1 keV c^{-2}, or $\sim 10^{-33}$ kg, about 500 times smaller than the mass of an electron.

A leading candidate for these massive neutrinos is the sterile neutrino (Dodelson & Widrow, 1994), a hypothetical particle whose existence would explain a number of surprising properties of ordinary neutrinos. Being able to solve two problems with one particle is a property that is shared among the most popular dark-matter candidates, because it provides more reason to believe in this theory than in some ad-hoc postulated particle. One such theory, called supersymmetry (Gervais & Sakita, 1971; Gol′fand & Lihtman, 1971; Volkov & Akulov, 1972; Wess & Zumino, 1974), is a proposed extension of the standard model of particle physics that would explain why gravity is very weak compared to other forces (Dimopoulos & Georgi, 1981). Several supersymmetric particles collectively known as neutralinos fit the description of a WIMP and the requirements of a dark-matter particle (e.g. Ellis et al., 1984). Another theory, quantum chromodynamics (Fritzsch et al., 1973), is part of the standard model, but has a hard to explain feature, known as the strong CP problem (Belavin et al., 1975; Callan et al., 1976; Jackiw & Rebbi, 1976; Polyakov, 1975; 't Hooft, 1976a,b). Axions (Weinberg, 1978; Wilczek, 1978) and axion-like particles (ALPs; Abbott & Sikivie, 1983; Dine & Fischler, 1983; Preskill et al., 1983) are another popular candidate, because their existence would naturally explain the strong CP problem.

Modern measurements of the cosmic microwave background (CMB; Dicke et al., 1965; Penzias & Wilson, 1965) – the earliest detectable emission in the Universe – and weak gravitational lensing with the *Planck* satellite, combined with external data, reveal that only ≈16% of the matter in the Universe is baryonic, while the rest is dark (Planck Collaboration, 2016)[3]. Together, matter forms only ≈31% of the energy budget of the Universe: ≈5% baryonic and ≈26% dark. The remaining ≈69% is well-described by the cosmological constant, Λ. The cosmological constant is a property of spacetime itself, making spacetime expand or contract depending on its value. It is responsible for the observed accelerating expansion of the Universe (Perlmutter et al., 1999; Riess et al., 1998). The cosmological constant

3. In this thesis I use the *Planck* 2015 cosmological parameters, which were the latest published results from the *Planck* satellite at the time when I started this research. The more recent *Planck* 2018 cosmological parameters (Planck Collaboration, 2020) are consistent with the previous ones, and identical when rounded to the precision given in the paragraph above.

is a working theory rooted in history[4] and the simplest explanation of the accelerated expansion. The accelerated expansion could alternatively be caused by adding a new form of energy to the contents of the Universe. This unknown ingredient is called dark energy, reflecting our lack of knowledge and mirroring the term dark matter. Even though Λ and CDM are both poorly understood, the ΛCDM model that they form is able to match large-scale observations of the Universe at an exquisite level, and has therefore become the leading paradigm in cosmology.

1.1.2 Small-scale problems

Despite the successes of ΛCDM on the large scales, reconciling the paradigm with observations at smaller scales has been more difficult (see Bullock & Boylan-Kolchin, 2017 for a review). On several fronts, differences were found between the observed population of Milky Way satellite galaxies and the expectations from the earliest CDM simulations. The debate whether the discrepancies are due to CDM being wrong, or these simulations being incomplete, is still ongoing. The earliest simulations did not account for baryons; including baryons and baryonic physics may solve or alleviate at least some of these problems. In this Section I will present the three small-scale problems that have received the most attention in the literature, which are also the three that are most relevant to this thesis.

The small-scale problem that is central to the work presented in this thesis, is the cusp–core problem. In early simulations of the formation of dark-matter structures in the Universe, it was found that the dark-matter haloes that would presumably host the galaxies and galaxy clusters had a cuspy density profile that keeps rising as one gets closer to the centre of the halo ($\rho(r) \propto r^{-1}$ as $r \to 0$; Dubinski & Carlberg, 1991; Navarro et al., 1996b). Several classical dwarf galaxies, on the other hand, were observed to be hosted by cored dark-matter haloes, where the density profile becomes constant in the centre ($\rho(r) \propto r^0$ as $r \to 0$; Flores & Primack, 1994; Moore, 1994). At first sight, this discrepancy seems to rule out CDM, but it is important to consider the effects of baryons on the inner profiles.

Another prediction of early dark-matter simulations is that many more smaller haloes will be formed than larger haloes will be, and that there is no cut-off mass below which no more haloes are formed (Ghigna et al., 1998; Klypin et al., 1999a). This halo mass function would mean that there

4. Einstein (1917) initially proposed a cosmological constant, positive but smaller than today's value, to balance the gravitational forces of matter and prevent the collapse of the Universe, making it static. When Hubble (1929; see also Lemaître 1927) showed that the Universe is in fact expanding, Einstein (1931) abandoned the cosmological constant.

should be thousands of dark-matter haloes around the Milky Way that are in principle massive enough to host a galaxy. In contrast, there are less than a hundred confirmed or candidate Milky Way satellites (Klypin et al., 1999b; Moore et al., 1999). Either significantly fewer dark-matter haloes have been formed than predicted by CDM, or galaxy formation is very inefficient at low halo masses. This problem is known as the missing satellites problem.

The last of the three most-discussed small-scale problems is that the most massive observed satellite galaxies have haloes with central densities lower than those of the most massive satellite haloes in CDM simulations (Boylan-Kolchin et al., 2011). These findings suggest that the most massive dark-matter haloes do not form galaxies, while lower-mass haloes do. This problem is called the too-big-to-fail problem, because more massive haloes are expected to form galaxies more easily; the massive haloes are too big to fail to form a galaxy. Again, the question is whether adding baryons will alleviate this tension, or if the ΛCDM paradigm is in trouble.

1.1.3 Baryonic effects

The first cosmological simulations assumed CDM was the only matter in the Universe. This may seem a fair approximation given the energy budget of the Universe, but baryons play an important role in the centres of galaxies, where they can be more abundant than dark matter.

In massive galaxies, which contain relatively large amounts of baryons, the more centrally concentrated baryons have an effect on the dark-matter distribution due to their gravitational attraction. In what is known as baryonic contraction, the presence of the baryons increases the central density of dark matter (Blumenthal et al., 1986). As a result, the dark-matter density profile of massive galaxies is even steeper than $\rho(r) \propto r^{-1}$ as $r \to 0$. The increased steepness would counteract any process that creates a central core. Unfortunately, this means that the central density profiles of the galaxies that are most easily studied are unsuited for constraining the nature of dark matter.

At the dwarf-galaxy scale, star-formation feedback takes over from baryonic contraction. When massive stars die in a supernova, a large amount of energy is released into the surrounding material, consisting mostly of gas (Navarro et al., 1996a). With repeated supernovae, the gas is heated and blown to larger radii, where it will subsequently cool and re-accrete (Pontzen & Governato, 2012). As a result, the gas mass within the half-light radius – the radius from wherein half of the galaxy's light is emitted, and the relevant scale for the stellar population – will fluctuate. Even though the interaction between baryons and CDM particles is thought to be non-existent, the fluctuations in the central gas mass will affect the distribution of dark

matter through gravity. Specifically, the lowered central mass – or equivalently, the increased mass at large radii – causes some of the dark matter to flow towards larger radii, thereby reducing the inner dark-matter density and flattening the cusp. Through this process, star formation feedback would address both the cusp–core problem and the too-big-to-fail problem. Furthermore, in the smallest dwarf galaxies, star-formation feedback could blow out most of the gas after the first round of star formation. These galaxies are then extinguished, which could explain the missing satellites problem.

Star formation feedback is therefore an interesting effect that could resolve the three major small-scale problems of ΛCDM. Regardless, it will have an impact on the predictions of ΛCDM and must therefore be included in the simulations. Adding star formation feedback is unfortunately not straightforward, because in a cosmological simulation (e.g. Schaye et al., 2015), simulating the life cycle of every star in every galaxy, including its effects on surrounding gas, is far beyond the computational capabilities of the present. Instead of simulating stellar evolution, its effects are addressed with subgrid recipes (e.g. Crain et al., 2015). Such a recipe is a set of rules, such as: if the gas density reaches a threshold, stars are formed, and after a predefined amount of time, a predefined amount of energy will be released to mimic a supernova. Simulations focusing on smaller volumes with only a few galaxies e.g. Hopkins et al., 2014, or on single isolated galaxies, can afford to use higher spatial resolutions. Such simulations now show that the cores of dwarf galaxies can indeed be explained with star formation feedback (Oñorbe et al., 2015; Read et al., 2016). Furthermore, it has recently been shown that the core sizes of observed dwarf galaxies correlate with the amount of star formation they have experienced (Read et al., 2019). It is therefore possible that the most common small-scale problems are resolved with more realistic simulations that account for additional physics.

1.1.4 Alternatives to CDM

Prompted by the failure of dark matter–only simulations to reproduce the observed structure in the Universe, several alternatives to CDM have been proposed. In the discussion of the ΛCDM paradigm, it was already mentioned that HDM has historically been considered, but subsequently ruled out. This Section lists a few popular alternatives that are still actively studied.

Though HDM was ruled out by simulations that found it produced too tenuous structure, warm dark matter (WDM; Bode et al., 2001) is still possible. The mass of WDM particles is in between that of CDM and HDM particles. It should form structures similar to CDM, but at the smallest scales

the lower mass will form slightly lower peaks in the density. This could explain the cores in dwarf galaxies, and would also solve the missing satellites and too big to fail problems by erasing the smaller dark-matter haloes. An example of a proposed WDM particle is the sterile neutrino.

Self-interacting dark matter (SIDM), which has an interaction between dark-matter particles that is stronger than that between a dark-matter particle and a non–dark-matter particle, is another popular option. There are two variations of SIDM: the interaction could result in scattering (Spergel & Steinhardt, 2000) or annihilation (Kaplinghat et al., 2000). Scattering SIDM is often simply known as SIDM. The scattering interaction results in an exchange of energy, which slowly equalizes the distribution of energy among the particles. The effect is strongest in the regions with the highest dark-matter density, where more collisions happen. As a result, the density of a halo becomes constant in the centre. In annihilating SIDM, colliding dark-matter particles convert into non–dark-matter particles. This similarly results in a reduction of the central density towards a constant value. The constant central densities of both variations of SIDM directly address the cusp–core problem. Similar to WDM, the missing satellites and too big to fail problems are addressed through the erasure of the densest structures.

Lastly, a lowering of the central density could also be achieved by assuming dark matter is made of extremely light bosons, with masses of $\sim 10^{-22}\,\mathrm{eV}\,c^{-2}$, or $\sim 10^{-58}\,\mathrm{kg}$ (Hu et al., 2000). Ultra-light ALPs fit this description, but are not the only possibility (e.g. Ferreira, 2021). This kind of dark matter, known as fuzzy dark matter (FDM), relies on quantum mechanics to solve the small-scale problems. In quantum mechanics, matter behaves like a wave at small scales. A quantum of matter, which we classically think of as a particle that can be pinpointed to a location, is in fact more diffuse. The 'fuzziness' of matter is characterizedby its de Broglie (1925) wavelength. This wavelength will be on the order of $10\,\mathrm{kpc}$ ($\approx 3 \times 10^{20}\,\mathrm{m}$) for the aforementioned FDM mass scale and a velocity typical of a particle in a dwarf galaxy ($\sim 10\,\mathrm{km\,s^{-1}}$). At scales below the de Broglie wavelength, quantum mechanical effects start to become significant. The collapse of structure is halted by Heisenberg's uncertainty principle (Heisenberg, 1927), which limits how close particles can be in location and momentum. The result is a 'quantum pressure' that counters gravity and creates a structure known as a soliton, which also has a constant-density core. Extensions to FDM exist, for example through the addition of self-interaction, and the overarching theory is called scalar-field dark matter (SFDM; e.g. Rindler-Daller, 2021) or ultra-light dark matter (UFDM; e.g. Ferreira, 2021). Even more generally, wave dark matter (e.g. Hui, 2021) includes heavier particles, up to $\sim 30\,\mathrm{eV}\,c^{-2}$, or

$\sim 5 \times 10^{-35}$ kg, that still behave more like waves than like classical particles, though these particles will not solve the small-scale problems.

These alternative theories add extra properties to dark matter to achieve the observed behaviour. These extra properties are also their biggest fundamental weakness: with baryonic feedback we can describe the observations without additional physics, but these alternative theories often ascribe new interactions to dark matter. As scientists generally prefer the simplest theory that can explain the observations, the alternative theories will have to outperform CDM with baryonic feedback, or will need external corroboration, before we will be willing to accept them as true.

1.1.5 Alternatives to dark matter

Though ΛCDM is currently the leading cosmological paradigm, not all astronomers are convinced. The most popular alternative to ΛCDM is modified Newtonian dynamics (MOND; Milgrom, 1983a,b,c). In MOND, the discrepancy between the expectation from luminous matter and the observations, of velocity dispersions in clusters of galaxies and of rotational velocities in the outskirts of galaxies, are interpreted as evidence for an alternate law of gravity instead of additional mass. The modification of gravity would have to become only apparent at large scales, where forces and accelerations are small, and must reproduce the established behaviour at small scales. This idea is similar to relativity, which only starts to deviate noticeably from Newtonian gravity when velocities reach an appreciable fraction of the speed of light.

With MOND the rotation curves of galaxies can be explained very well, but in its original form it struggles to explain the large-scale observations of the Universe, such as the CMB, where ΛCDM works best. The original form is also an ad-hoc theory, though the same can be said of the origins of CDM. More problematically, the original MOND violates the conservation of energy, momentum, and angular momentum, which are established principles of physics, and does not conform to the theory of general relativity. If MOND is proven correct, we would therefore have to rewrite a large part of physics.

Since the original proposals, several attempts have been made to arrive at a MOND-like theory that does not break established physics. The currently most successful version is tensor–vector–scalar gravity (TeVeS; Bekenstein, 2004). This theory is much more complex and therefore more flexible than the original MOND, which makes it easier to reconcile it with different observations. On the other hand, the elegant simplicity and predictiveness, which attracted many to MOND, is largely lost.

1.2 Where to study dark matter

There are several strategies to studying dark matter, which can complement each other. Perhaps the most obvious study targets are galaxy clusters. These structures have the largest amounts of dark matter, therefore it should be easier to achieve a detection. The main method used for studying dark matter in galaxy clusters is to look for annihilation or decay signals. Though the dark matter itself is invisible, if the particles can interact with each other, or if they are unstable, visible reaction products may be formed. These are most often sought in the form of cosmic γ rays e.g. Fermi LAT collaboration, 2015; Gunn et al., 1978; Stecker, 1978 or X rays (e.g. Abazajian et al., 2001; Boyarsky et al., 2014; Bulbul et al., 2014), but searches for antiprotons and positrons are also performed (e.g. Adriani et al., 2010; AMS Collaboration, 2013; Silk & Srednicki, 1984). The energies of these cosmic rays are related to the mass of the dark-matter particle. A detection of an annihilation or decay signal would therefore provide us with crucial information regarding the nature of dark matter. Though no signals have been conclusively detected, their absence places constraints on the properties of dark matter. Galaxy clusters have an additional benefit in that they not only contain large quantities of dark matter in an absolute sense, but also in a relative sense. Their strongly dark matter–dominated nature reduces the potential for confusing a baryonic emission line for a dark-matter one, and lowers the background noise level.

Another option is to search for the same annihilation or decay signatures in massive individual galaxies. Though these galaxies do not contain as much dark matter as galaxy clusters, there are several that are in close proximity to us, including our own Milky Way. This proximity would result in relatively high fluxes, even if the initial luminosity is lower. The downside of using massive galaxies is that they are not as dark matter–dominated as galaxy clusters. A significant excess of γ rays has been detected coming from the direction of the centre of the Milky Way (Goodenough & Hooper, 2009). It is, however, not clear whether this emission is caused by dark matter, or by something baryonic, such as pulsars (Abazajian, 2011).

Moving further down in mass, dwarf galaxies are again a very suitable target. Dwarf galaxies are very dark matter–dominated and while they contain much less dark matter than galaxy clusters, they can be found much more nearby. Thanks to these properties, very strong constraints on dark-matter annihilation can be placed using dwarf galaxies (e.g. Albert et al., 2020; Fermi-LAT Collaboration, 2015; H.E.S.S. Collaboration, 2020; MAGIC Collaboration, 2022; VERITAS Collaboration, 2017). As discussed in Sect. 1.1.2, dwarf galaxies are also in the regime where dark-matter density profiles start to become cored instead of cuspy. This transition could

be a sign of dark-matter physics beyond CDM, but it could also be due to baryonic feedback. If the latter is true, it is expected that the faintest, lowest-mass, and most dark matter–dominated dwarf galaxies, called ultra-faint dwarf galaxies (UFDs), will again have cuspy dark-matter density profiles (e.g. Oñorbe et al., 2015; Peñarrubia et al., 2012; Wheeler et al., 2019). The density profiles of UFDs are therefore an important piece of information to resolve the debate regarding the cusp–core problem, but none had been constrained at the time when work on this thesis commenced.

One can go even closer to home, by considering that the Solar system is embedded in the dark-matter halo of the Milky Way. Dark-matter particles should therefore be whizzing past and through us while we sweep out our orbit. If dark matter has a non-zero interaction cross section, every once in a while a dark-matter particle may collide with a baryonic particle and deposit energy. Nuclear recoil experiments use this effect by monitoring a large mass, usually a liquid noble gas, for unexplained energy depositions (e.g. Ahlen et al., 1987; XENON Collaboration, 2018). Furthermore, the Sun, and even the Earth, may host their own haloes of gravitationally captured dark matter (Freese, 1986; Krauss et al., 1985; Silk et al., 1985). The dark-matter particles may annihilate into neutrinos, which are searched for using neutrino telescopes (e.g. AMANDA Collaboration, 2002; ANTARES collaboration, 2013; IceCube Collaboration, 2013; Super-Kamiokande Collaboration, 2004). Finally, if dark matter consists of axions or ALPs, local dark-matter particles may be detected using a resonant microwave cavity (e.g. Asztalos et al., 2004; Brubaker et al., 2017; DePanfilis et al., 1987; Sikivie, 1983). Axions and ALPs can convert into photons under the influence of a strong magnetic field. The conversion is most efficient when the resonance frequency of the cavity matches the dark-matter particle mass, thereby making it possible to constrain the mass of axions and ALPs as well.

1.3 Ultra-faint dwarf galaxies

From the previous Sections it is apparent that UFDs are a particularly interesting target for studying the properties of dark matter. The inner density profiles of UFDs can be used to distinguish between CDM and its alternatives, and answer whether the cores of the more massive dwarf galaxies are caused by baryonic or dark-matter physics. Furthermore, UFDs can be used to constrain the annihilation and decay of dark matter, but accurate density profiles are necessary to arrive at accurate constraints through this method. In this thesis, I therefore focus on determining the density profiles of UFDs, and the constraints on dark matter that can be obtained from them. I summarize our knowledge of UFDs below; a more complete review was recently given by Simon (2019).

FIGURE 1.1: Composite-colour image of the UFD Eridanus 2 from DES Data Release 2 (DES Collaboration, 2015c, 2018; DES Collaboration et al., 2021), using i, r, and g colours for the red, green, and blue channels, respectively. Eridanus 2 was discovered in earlier data from DES. The UFD is visible as a resolved cloud of bluish stars, approximately covering the *central ninth* of the image, and has a higher stellar number density than the foreground distribution of Milky Way stars. Near the centre of the UFD, the star cluster of Eridanus 2 is visible as an even denser cloud of bluish stars, next to a bluish background galaxy.

A UFD is simply a dwarf galaxy that is extremely faint – specifically, defined as having an absolute V-band magnitude $M_V > -7.7$ (Simon, 2019). There is no physical significance to this dividing line in luminosity, but it corresponds to the approximate limit of analogue astronomical detection methods. The discovery of UFDs was made possible with the introduction of digital image sensors in astronomy, which allow to capture much fainter objects. The first UFD to be discovered is, in retrospect, Willman 1 (Willman et al., 2005), found in the data of the Sloan Digital Sky Survey (SDSS; York et al., 2000). It took several years to interpret the properties of this new and puzzlingly faint object with enough confidence to claim it is a galaxy as opposed to a star cluster (Willman et al., 2011). More recently, a large number of UFDs (e.g. DES Collaboration, 2015a; Koposov et al., 2015) have been found in the Dark Energy Survey (DES; example shown in Fig. 1.1; Abbott et al., 2005), as well as using several dedicated programmes (e.g. DELVE Collaboration & Astro Data Lab, 2021; Nidever et al., 2017). Due to their faintness, most UFDs that have been found are satellites of the Milky Way or possibly the Magellanic Clouds, though several have been detected around the neighbouring galaxy Andromeda, and a few ultra-faint objects have been sighted outside of the Local Group (Simon, 2019).

As UFDs are galaxies, they are distinct from ultra-faint star clusters in that they are hosted in a dark-matter halo (Simon, 2019). The dark-matter haloes impart a significant velocity dispersion on the stars (e.g. Kleyna et al., 2005; Muñoz et al., 2006), as well as a metallicity dispersion (e.g. Martin et al., 2007; Muñoz et al., 2006; Simon & Geha, 2007), indicative of having an extended star formation history and enough mass to bind some of the metal-enriched supernova ejecta. The half-light radii of UFDs, ranging from $\approx$10 to $\approx$300 pc ($\approx 3 \times 10^{14}$ to $\approx 1 \times 10^{16}$ km; Simon, 2019), are typically larger than those of star clusters of the same luminosity, though the faintest UFDs and star clusters can be very hard to distinguish. These sizes are equivalent to one to several arcminutes on the sky, densely populated with stars. The metallicities of UFDs are very low, $[\mathrm{Fe/H}] \lesssim -2$ (e.g. Martin et al., 2007; Muñoz et al., 2006; Simon & Geha, 2007), and follow a metallicity–luminosity relation (Kirby et al., 2013, 2008; Simon & Geha, 2007). In contrast, star clusters do not follow a metallicity–luminosity relation. To classify an ultra-faint satellite as a UFD or a star cluster, it is generally necessary to determine its kinematics or metallicity. Both determinations require spectroscopy, which is challenging for such faint systems. A large number of candidate UFDs are hence still awaiting spectroscopic confirmation (Simon, 2019).

Due to their relatively recent discovery and how challenging they are to

observe, there are plenty of yet unanswered questions regarding UFDs. I have discussed the question of their density profiles before, the determination of which depends on the assumption of dynamical equilibrium. Whether UFDs are in equilibrium, and whether they are galaxies at all, is questioned by some. Most UFDs are found close to their pericentre, where galaxies spend the least amount of time along their orbit (Simon, 2018). In has been proposed that UFDs are instead tidally shocked or stripped remnants, their large velocity dispersions being created by disequilibrium instead of dark matter (e.g. Hammer et al., 2018). On the other hand, the pericentre locations could be due to observational bias, which would mean that a much larger number of UFDs is currently lurking at larger distances, too faint to detect with current instruments (Simon, 2019). Furthermore, while the total velocity at the pericentre is maximal, the radial velocity is zero, therefore a satellite galaxy will spend a relatively large amount of time near its minimum galactocentric radius (Pace et al., 2022). The stellar properties of UFDs are also an active area of research. Not much is known yet about the population of binary stars in UFDs – what their periods are, and what the binary fraction is – though several individual binary systems have been discovered (e.g. Frebel et al., 2010; Koch et al., 2014; Koposov et al., 2011). Spectroscopic observations aimed at determining stellar kinematics need to take these unknowns into account in the survey design, or else the velocity dispersion may be biased (McConnachie & Côté, 2010; Spencer et al., 2017b). The binaries, as well as the distribution of stellar masses, will also be able to tell us something about star formation in these galaxies. The very metal-poor nature of these galaxies provides a way to test whether the initial mass function is metallicity-dependent (e.g. Geha et al., 2013; Gennaro et al., 2018a,b). In general, UFDs are a new regime that we can use to test our understanding of star formation. The smallest UFDs are thought to be at the edge of star formation and are therefore very sensitive to galaxy formation physics (e.g. Kravtsov, 2003; Saitoh et al., 2008). The limits of star formation will also inform us about the faint end of the galaxy luminosity function and the stellar–halo mass relation. The above questions are all interesting research topics, but cannot all be addressed in this thesis. The focus of this thesis is therefore on the density profiles, due to their ability to constrain the nature of dark matter, as well as on tidal stripping and the stellar–halo mass relation, which can be determined from the density profiles and the already available photometric observations.

1.4 Dynamics

In Sect. 1.1.1 I already introduced that there is a relation between the mass distribution of a system (e.g. a galaxy) and the motions of the particles (e.g.

stars) in that system. In this Section I will make this connection more concrete.

The motion of stars in the plane of the sky, called proper motion, is generally too slow to discern a change in position of a star in a different galaxy, even for relatively nearby ones. It has only become possible very recently to measure the internal proper motions of some of the brightest satellites of the Milky Way, by comparing the positions of stars over a decade-long baseline (Massari et al., 2018, 2020). Such measurements are still out of reach for the much fainter and more recently discovered UFDs. It is therefore necessary to focus on the motions along the line of sight, which can be measured using the Doppler (1842) effect. In this Section I will introduce the connection between the mass distribution and the line-of-sight velocities (Sect. 1.4.1) and how these velocities can be measured using the Doppler effect (Sect. 1.4.2)

The following material, especially Sect. 1.4.1, will necessarily be more mathematical and technical in nature than the previous pages. If the reader is content with the high-level overview of the previous paragraph and not interested in the underlying details, they may skip ahead to Sect. 1.4.2.

1.4.1 Jeans equations

Let $\Phi(\boldsymbol{x}, t)$ be the gravitational potential of the system and $\nu(\boldsymbol{x}, t)$ the number density of the tracers of the potential (i.e. the stars). Both are functions of the three-dimensional position $\boldsymbol{x} = (x_1, x_2, x_3)$ and of time t. Using the indices i and j to refer to vector and matrix elements, the velocities of the tracers are denoted $v_i(\boldsymbol{x}, t)$ and their first and second raw moments are $\overline{v}_i(\boldsymbol{x}, t)$ and $\overline{v_{ij}^2}(\boldsymbol{x}, t) \coloneqq \overline{v_i(\boldsymbol{x}, t) v_j(\boldsymbol{x}, t)}$, where $\overline{\ldots}$ denotes an average over the ensemble of tracers, while the velocity covariance is denoted with $\sigma_{ij}^2(\boldsymbol{x}, t)$.

The relation between $\Phi(\boldsymbol{x}, t)$, $\nu(\boldsymbol{x}, t)$, and the velocity moments is described by the Jeans equations (Clerk Maxwell, 1867; Jeans, 1915). Using Einstein (1916) notation, wherein repeated indices in a single term are summed over (e.g. $a_i b_i = a_1 b_1 + a_2 b_2 + a_3 b_3$), the Jeans equations can be written as (Binney & Tremaine, 2008)

$$\frac{\partial \nu(\boldsymbol{x}, t)}{\partial t} + \frac{\partial\big(\nu(\boldsymbol{x}, t)\overline{v}_i(\boldsymbol{x}, t)\big)}{\partial x_i} = 0, \tag{1.1}$$

$$\begin{aligned} \nu(\boldsymbol{x}, t)\frac{\partial \overline{v}_j(\boldsymbol{x}, t)}{\partial t} + \nu(\boldsymbol{x}, t)\overline{v}_i(\boldsymbol{x}, t)\frac{\partial \overline{v}_j(\boldsymbol{x}, t)}{\partial x_i} = \\ - \nu(\boldsymbol{x}, t)\frac{\partial \Phi(\boldsymbol{x}, t)}{\partial x_j} - \frac{\partial\big(\nu(\boldsymbol{x}, t)\sigma_{ij}^2(\boldsymbol{x}, t)\big)}{\partial x_i}. \end{aligned} \tag{1.2}$$

The first of these equations is a continuity equation. It simply means that a change in the tracer number density at a certain point in space is accompanied by an equivalent in- or outflow of tracers. In other words, the 'fluid' of tracers is not created or destroyed, it just moves around. The second equation, the momentum equation, is more interesting in the context of measuring mass, because it contains the gravitational potential.

In this thesis I use existing pieces of software, CJAM (Watkins et al., 2013) and (py)GravSphere (Collins et al., 2021; Genina et al., 2020; Read & Steger, 2017; Read et al., 2018), that are specifically designed to solve the second Jeans equation. Given a mass distribution and a tracer distribution, they predict the observed velocity dispersion, which can be compared against the measurements. To arrive at a unique solution, further assumptions have to be made. Due to the complexity of the equations, I will illustrate this process using one set of assumptions that yield a relatively simple solution.

First, I assume that the system is in equilibrium. Therefore, $\partial/\partial t = 0$ and $\partial/\partial x_i = \mathrm{d}/\mathrm{d}x_i$. I further assume the system is spherically symmetric and non-rotating, and describe it with the radial coordinate r, polar coordinate θ, and azimuthal coordinate ϕ. Due to the spherical symmetry, quantities are only dependent on the radius, so $\partial/\partial r = \mathrm{d}/\mathrm{d}r$, $\partial/\partial\theta = 0$, and $\partial/\partial\phi = 0$. The lack of rotation means that $\overline{v}_\theta = 0$ and $\overline{v}_\phi = 0$. Furthermore, $\overline{v}_r = 0$, because otherwise the system would collapse or dissolve, which is not consistent with the assumption of equilibrium. As a result, $\sigma^2_{rr} = \overline{v^2_{rr}}$, $\sigma^2_{\theta\theta} = \overline{v^2_{\theta\theta}}$, and $\sigma^2_{\phi\phi} = \overline{v^2_{\phi\phi}}$. The second Jeans equation then simplifies to (Binney & Tremaine, 2008)

$$\frac{\mathrm{d}\big(\nu(r)\sigma^2_{rr}(r)\big)}{\mathrm{d}r} + \nu(r)\left(\frac{\mathrm{d}\Phi(r)}{\mathrm{d}r} + \frac{2\sigma^2_{rr}(r) - \sigma^2_{\theta\theta}(r) - \sigma^2_{\phi\phi}(r)}{r}\right) = 0. \tag{1.3}$$

It is customary to introduce the velocity anisotropy (Binney & Tremaine, 2008),

$$\beta(r) \coloneqq 1 - \frac{\sigma^2_{\theta\theta}(r) + \sigma^2_{\phi\phi}(r)}{2\sigma^2_{rr}(r)}, \tag{1.4}$$

which describes whether there is a preferred direction in the kinematics. If $\beta = 0$, the velocity is isotropic, meaning there is no preferred direction. The two extremes are $\beta = 1$, when all motions are radial, and $\beta \to -\infty$, when all motions are tangential (i.e. polar or azimuthal, or a combination thereof). With the velocity anisotropy, the spherical Jeans equation can be written as

$$\frac{\mathrm{d}\big(\nu(r)\sigma_{rr}^2(r)\big)}{\mathrm{d}r} + 2\frac{\beta(r)}{r}\nu(r)\sigma_{rr}^2(r) = -\nu(r)\frac{\mathrm{d}\Phi(r)}{\mathrm{d}r} = -\nu(r)\frac{GM(<r)}{r^2}, \quad (1.5)$$

wherein I have introduced the mass $M(<r)$ enclosed in a radius r from the centre of the system. If the velocity anisotropy is constant with radius, this equation is relatively easy to solve for the radial velocity dispersion (Binney & Tremaine, 2008),

$$\sigma_{rr}^2(r) = \frac{1}{r^{2\beta}\nu(r)}\int_r^\infty r'^{2\beta}\nu(r')\frac{\mathrm{d}\Phi}{\mathrm{d}r'}\,\mathrm{d}r'. \quad (1.6)$$

To convert from these internal velocity dispersions to the ones observed, we need to change variables. Let x and y be the coordinates on the plane of the sky, and z the coordinate perpendicular to that plane. The velocity dispersion that we observe is the one along the line of sight, in the direction of z. As we look through the galaxy along the line of sight, we probe different three-dimensional locations in the galaxy. The velocity dispersion in the z direction must therefore be integrated along the line of sight and weighted with the tracer number density:

$$\sigma_{\mathrm{los}}^2(x,y) = \frac{\int_{-\infty}^{+\infty}\nu(x,y,z)\sigma_{zz}^2(x,y,z)\,\mathrm{d}z}{\int_{-\infty}^{+\infty}\nu(x,y,z)\,\mathrm{d}z}. \quad (1.7)$$

Because we have assumed a spherical symmetry, we can replace the coordinates on the plane of the sky with the projected radius $R = \sqrt{x^2+y^2}$. Being free to choose the polar and azimuthal directions without loss of generality, we can substitute

$$\sigma_{zz}^2(r) = \sigma_{rr}^2(r)\sin^2\phi + \sigma_{\phi\phi}^2(r)\cos^2\phi = \sigma_{rr}^2(r)\frac{r^2-R^2}{r^2} + \sigma_{\phi\phi}^2(r)\frac{R^2}{r^2}, \quad (1.8)$$

introduce β from Eq. 1.4, and change variables to get

$$\sigma_{\mathrm{los}}^2(R) = \frac{2}{\Sigma_*(R)}\int_R^\infty \nu(r)\left(1-\beta\frac{R^2}{r^2}\right)\sigma_{rr}^2(r)\frac{r}{\sqrt{r^2-R^2}}\,\mathrm{d}r, \quad (1.9)$$

where

$$\Sigma_*(R) = \int_{-\infty}^{\infty}\nu(x,y,z)\,\mathrm{d}z = 2\int_R^\infty \nu(r)\frac{r}{\sqrt{r^2-R^2}}\,\mathrm{d}r \quad (1.10)$$

is the stellar number surface density at the projected radius R.

There are two ways in which $\sigma_{\mathrm{los}}^2(R)$ can be compared against the measurements. One is to calculate the variance of the measured line-of-sight velocities in bins of R. This method is the easiest, but in the binning process,

information is lost. A binned analysis will therefore not have as much constraining power on the mass distribution as it could have, unless it is combined with additional estimators, such as virial shape parameters (Merrifield & Kent, 1990), to make up for the lost information. Another approach is to compare each individual line-of-sight velocity measurement against the expected distribution. The expectation value of the line-of-sight velocity is the ν-weighted average of $\overline{v}_z(r)$ along the line of sight, which is the systemic velocity in the case presented here, while the intrinsic variance of the expected velocities is $\sigma^2_{\rm los}(R)$. The observed variance will be inflated by the measurement uncertainties ε:

$$\sigma^2_{\rm los,obs} = \sigma^2_{\rm los} + \varepsilon^2. \tag{1.11}$$

If it is assumed that the line-of-sight velocities are normally distributed according to these expected moments, the mass distribution can be constrained without losing information. In theory, this last method could be improved by adding higher moments to the comparison between the measurements and the expected distributions. However, for this thesis there is little to gain from such an exercise given that the constraints on the mass distributions of UFDs are dominated by the relatively large measurement uncertainties and small numbers of stars.

1.4.2 Spectroscopy

If a star has a non-zero line-of-sight velocity, its emissions are affected by the Doppler (1842) effect. A photon emitted with wavelength λ_0 will be observed as having a wavelength

$$\lambda_{\rm obs} = \lambda_0(1 + z), \tag{1.12}$$

where z is the spectroscopic redshift of the star. In the non-relativistic limit, the redshift is given by

$$z \approx \frac{v_{\rm los}}{c}, \tag{1.13}$$

where $v_{\rm los}$ is the line-of-sight velocity of the star, positive if the star is receding and negative if approaching, and c is the speed of light.

Due to the Doppler effect, characteristic features in the stellar spectra, such as the first two Balmer absorption lines Hα and Hβ, will shift in wavelength. By measuring the size of the shift, one can measure the line-of-sight velocity and from there the mass distribution of the galaxy. To be able to constrain the mass distribution strongly enough, one needs to measure the spectra of many stars with a spectral resolution high enough to resolve the expected line-of-sight velocity dispersion.

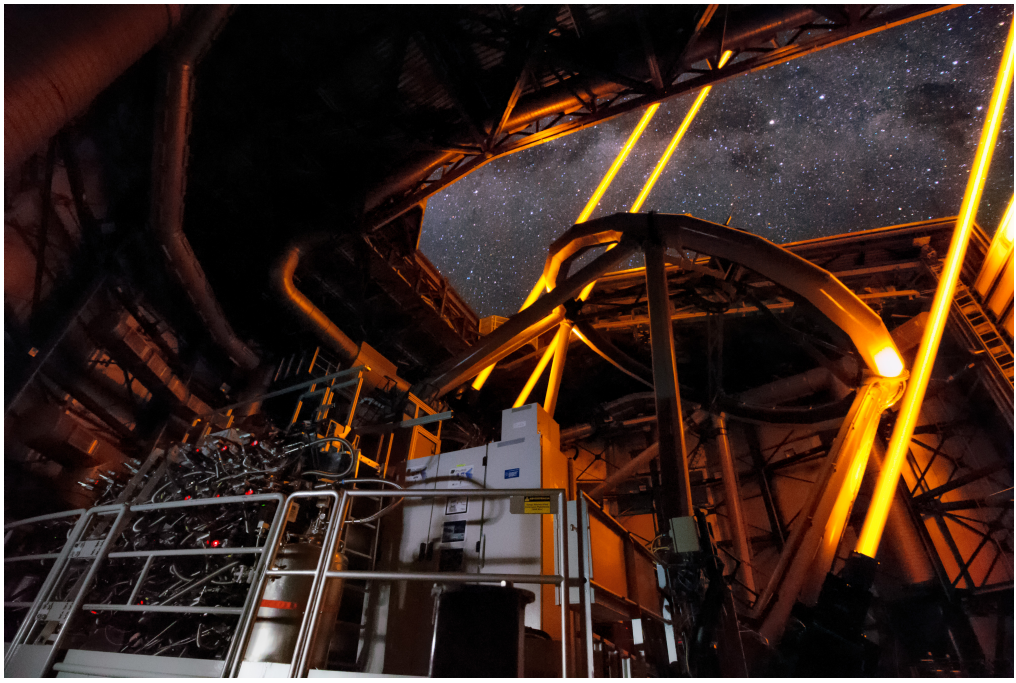

FIGURE 1.2: Photograph of MUSE (*bottom left, foreground*), mounted on UT4 of the VLT. The many cables and tubes connect the 24 integral-field units, each providing integral-field spectroscopy for a 24th part of the field of view, to the data acquisition, control, cooling, and vacuum systems. The AO lasers are mounted on the telescope support structure and shining out of the telescope dome towards the sky. The deformable secondary mirror is suspended inside the circular structure at the top end of the telescope support structure. The primary mirror is located at the bottom end of the telescope support structure, behind MUSE, and is not visible in this image. Image credit: Roland Bacon/ESO.

1.5 THE MUSE-FAINT SURVEY

Reviewing the above, to constrain the inner dark-matter density profiles of UFDs we need spectroscopic observations within their half-light radii, meaning an area of several square arcminutes, with high enough spatial resolution to separate the densely populated centres into their individual stars, and high enough spectral resolution to determine the stellar velocities with enough precision such that we can resolve the intrinsic velocity dispersion. This list of requirements is not easy to satisfy, but the Multi Unit Spectroscopic Explorer (MUSE; see Fig. 1.2; Bacon et al., 2010) is up to this task. This instrument is mounted on Unit Telescope 4 (UT4, also known by the indigenous name Yepun) of the Very Large Telescope (VLT), a group of four 8-m class telescopes located on the summit of Cerro Paranal,

FIGURE 1.3: Composite-colour MUSE-Faint image of Eridanus 2, using SDSS i, r, and g colours for the red, green, and blue channels, respectively. This image is constructed from five MUSE pointings. The star cluster of Eridanus 2 is located in the *lower right quadrant of the centre pointing*. The image covers approximately the area with the half-light radius. See also Fig. 3.1.

a mountain in the Atacama Desert, Chile. Being an integral-field spectrograph, MUSE essentially takes images wherein for each spatial element a spectrum is measured. This feat is achieved by chopping the image into different slices and dispersing the light such that spectra will fall on the image sensor. Because many pixels on the image sensor are required to measure the spectrum for each spatial element, the number of spatial elements is relatively limited, and so is the spectral resolution when compared to a conventional spectrograph. In the case of MUSE, the image consists of ≈300 by ≈300 spatial elements, where there are ≈3000 spectral elements for each spatial element. With these specifications, MUSE offers a spatial resolution that is relatively large for an integral-field spectrograph, while still offering medium-resolution spectra. Its field of view of a square arcminute is very small compared to imaging instruments, but ideal for observing the centres of UFDs and larger than that of other existing integral-field spectrographs. To achieve the required spatial resolution, we use the adaptive optics (AO) system of UT4 to minimize the impact of atmospheric turbulence on the image quality. Four sodium lasers create an artificial point source in the atmosphere, which is observed with the AO system. Actuators continuously adjust the shape of the telescope's secondary mirror to correct for the distortion of the incoming light waves by the atmosphere, using the artificial point source as a reference. Due to the brightness of the sodium lasers, the part of the spectrum near the wavelength of the lasers is contaminated and unusable, and is therefore masked before analysis.

Using 100 hours of guaranteed observing time, part of the time granted to the MUSE Collaboration in return for the development of MUSE, the MUSE-Faint survey[5] has been set up to observe ten[6] faint and ultra-faint, confirmed and candidate, dwarf galaxies, and also the centre of the classical dwarf galaxy Sculptor (Scl). Where available, the MUSE-Faint observations are supplemented by public MUSE data of the same targets. As of May 2022, the initial observations have been completed and reduced for five faint or ultra-faint dwarf galaxies: Antlia B (Ant B), Leo T, Eridanus 2 (Eri 2; see Fig. 1.3), Hydra II (Hya II), and Grus 1 (Gru 1). After the initial observations of Gru 1 were completed, it was decided to observe it further to increase the depth and the number of detected stars. Since the start of the analysis of the first batch of five galaxies, observations have been completed for most of the other targets: Pisces II (Psc II), Columba I (Col I), Pictor 1 (Pic 1),

5. The name MUSE-Faint is supposed to invoke the names of two other MUSE Collaboration surveys, MUSE-Deep and MUSE-Wide, and was coined during a conversation that I had with fellow MUSE Collaboration member Sebastian Kamann in May 2019, during a MUSE Busy Week.

6. Initially, 20 targets were planned, but this number was scaled down to allow for deeper observations.

Eridanus 3 (Eri 2), and the centre of Scl, as well as the second round of observations of Gru 1. These observations have not yet been fully analysed. The remaining target, Phoenix 2 (Phe 2), requires further observations. The MUSE-Faint observations are scheduled to finish by March 2023.

In this thesis, the first results of the MUSE-Faint survey are presented, focusing on dark-matter constraints and based on up to five of the observed galaxies: Ant B, Leo T, Eri 2, Hya II, and Gru 1. The survey is motivated not only by the constraints UFDs can offer on the nature of dark matter, but also by many of the other science goals discussed in Sect. 1.3. More detailed studies of Ant B and Leo T, which address not only their kinematics and dark-matter constraints, but also their stellar and gas properties, are underway (Brinchmann et al. in prep.; Júlio et al. in prep.; Vaz et al. in prep.). Lastly, external collaborators are leading a project to use the MUSE-Faint data in an innovative way, constraining the properties of ALPs by searching for optical decay signals in the space between the stars (Regis et al., 2021). As the exploration of MUSE-Faint data has only just begun to pick up speed after the initial observation, reduction, and analysis efforts, and as more data are still coming in, it is to be expected that the MUSE-Faint survey will lead to more novel results, both with regards to dark matter and to UFDs themselves.

1.6 This thesis

This thesis contains four studies that I have conducted together with my co-authors. We have investigated the nature and properties of faint and ultra-faint dwarf galaxies using their stellar kinematics, mainly from the MUSE-Faint survey. The main focus is on comparing CDM, annihilating SIDM, and FDM, though MACHOs are also featured. Furthermore, we compare the dark-matter halo properties of UFDs against theoretical expectations. The following Chapters are presented in chronological order, and with the passage of time the sample of analysed data increases from the central part of one UFD to a set of five faint and ultra-faint dwarf galaxies observed within their half-light radii.

In Chapter 2, we present the first MUSE-Faint data, of the central square arcminute of the UFD Eri 2. Earlier photometric observations revealed a stellar overdensity, which may be a star cluster hosted by Eri 2. Theoretical work has shown that the survival of this star cluster constrains the abundance of MACHOs in an interesting mass range. We measured the line-of-sight velocities of stars in Eri 2, both in the putative cluster and in the bulk. The kinematics supports the classification of the stellar overdensity as a star cluster hosted by Eri 2. We consequently updated the theoretical constraints on MACHOs using our data.

In Chapter 3, we expand the study of Eri 2 with MUSE-Faint data out to its half-light radius, and supplement with literature spectroscopy at larger radii. From the kinematics we constrain the first inner density profile of a UFD. We place limits on how cuspy or cored the profile can be and convert these limits to constraints on the self-interaction rate and annihilation cross section of SIDM and on the particle mass of FDM. We also compare the overall evidence for CDM, SIDM, and FDM, and conclude that there is no significant difference, though there is a slight preference for FDM.

In Chapter 4, we analyse four additional faint and ultra-faint dwarf galaxies, Ant B, Leo T, Hya II, and Gru 1, bringing the total number to five, supplementing their new MUSE-Faint stellar line-of-sight velocities with literature data at larger radii. We constrain the inner dark-matter density profiles and rule out large cores, while finding a slight preference for FDM over CDM and SIDM, for each galaxy. The difference in evidence is however not significant, therefore none of the models can be ruled out. We further find that the UFDs are not significantly tidally stripped. Their conformity to the theoretically expected mass–concentration and stellar–halo mass relations is sensitive to the analysis tools, and can thus not be established without further research.

In Chapter 5, we use the same sample of five faint and ultra-faint dwarf galaxies in a joint analysis to constrain the nature and properties of dark matter. After revising the method of Chapter 3 to provide efficient and unbiased results on the dark-matter properties, we constrain the annihilation cross section per unit mass of SIDM and the particle mass of FDM that best describe the data of all five galaxies simultaneously, using only weak assumptions. Combined with results for more massive dwarf galaxies, we find a very strong constraint on the FDM particle mass. Even though we make weaker assumptions about the properties of FDM than previous studies, our constraint is among the strongest determined from UFDs.

Acknowledgements

Figure 1.1 used public archival data from the Dark Energy Survey (DES). Funding for the DES Projects has been provided by the U.S. Department of Energy, the U.S. National Science Foundation, the Ministry of Science and Education of Spain, the Science and Technology Facilities Council of the United Kingdom, the Higher Education Funding Council for England, the National Center for Supercomputing Applications at the University of Illinois at Urbana–Champaign, the Kavli Institute of Cosmological Physics at the University of Chicago, the Center for Cosmology and Astro-Particle Physics at the Ohio State University, the Mitchell Institute for Fundamental Physics and Astronomy at Texas A&M University, Financiadora de

Estudos e Projetos, Fundação Carlos Chagas Filho de Amparo à Pesquisa do Estado do Rio de Janeiro, Conselho Nacional de Desenvolvimento Científico e Tecnológico and the Ministério da Ciência, Tecnologia e Inovação, the Deutsche Forschungsgemeinschaft, and the Collaborating Institutions in the Dark Energy Survey.

The Collaborating Institutions are Argonne National Laboratory, the University of California at Santa Cruz, the University of Cambridge, Centro de Investigaciones Energéticas, Medioambientales y Tecnológicas–Madrid, the University of Chicago, University College London, the DES-Brazil Consortium, the University of Edinburgh, the Eidgenössische Technische Hochschule (ETH) Zürich, Fermi National Accelerator Laboratory, the University of Illinois at Urbana–Champaign, the Institut de Ciències de l'Espai (IEEC/CSIC), the Institut de Física d'Altes Energies, Lawrence Berkeley National Laboratory, the Ludwig-Maximilians Universität München and the associated Excellence Cluster Universe, the University of Michigan, the National Optical Astronomy Observatory, the University of Nottingham, The Ohio State University, the OzDES Membership Consortium, the University of Pennsylvania, the University of Portsmouth, SLAC National Accelerator Laboratory, Stanford University, the University of Sussex, and Texas A&M University.

Based in part on observations at Cerro Tololo Inter-American Observatory, National Optical Astronomy Observatory, which is operated by the Association of Universities for Research in Astronomy (AURA) under a cooperative agreement with the National Science Foundation.